Journal of Visualization, Vol. 3, No. 3 (2000) 211-220

Control of Boundary Layer on a Flat Plate by Means of Cavity Flow

Aoki, K.*1, Okanaga, H.*1 and Nakayama, Y.*2

*1 Tokai University, Department of Mechanical Engineering, School of Engineering, 1117 Kitakaname, Hiratsuka, Kanagawa 259-1292, Japan.
*2 Future Technology Research Institute, 3-56-2 Higashi-Oizumi, Nerima-ku, Tokyo 178-0063, Japan.

Received 6 November 1999.
Revised 9 May 2000.

***Abstract*:** This paper describes the control of boundary layer on a flat plate by means of cavity flow. In this study, classifying the shapes of cavities into circular arc, rectangle and triangle makes the discussion, and the depths of the cavities are changed systematically. It is made clear, by numerical calculations and experiments, what states of flow are shown in the internal parts of cavities and what kinds of influence are exerted to the boundary layers in the upstream and downstream flows.

As a result, the following facts are made clear. By taking up properly the depth ratios (k/c) of cavities complying with the individual cavity shapes, the boundary layer thickness in the flow upstream and downstream of the cavities can be controlled. Meanwhile with any of the cavities, the existence of the minimum boundary layer thickness $(\delta/\delta_m)_{min}$ is seen at a depth ratio.

***Keywords*:** cavity flow, boundary layer control, boundary layer thickness, visualization, RNG κ–ε model.

1. Introduction

In consideration of the fact that a phenomenon of the flow separating from the surface of a solid body increases the troubles including loss, the studies on boundary layer control have been made from various viewpoints about external or internal flows. For the examples of external flow, there are researches (1) on the structure of a turbulent boundary layer with surface roughness (Okajima et al., 1973), square slots (Perry et al., 1966; Townes and Sabersky, 1966) and d-type square cavities (Choi, K.-S. and Fujisawa, 1993) installed on the flat plate, (2) on the changes of drag and lift by dimples applied on a sphere (Aoki et al., 1998), (3) on flow separation associated with a step or a groove (Tani et al., 1961) and (4) on turbulent drag reduction by riblets attached on a wall (Choi, K.-S., 1989) or a wing of an aircraft (Aihara et al., 1991), etc. Related to these researches, the flow inside rectangular and other cavities in a wall has been investigated (Maull and East, 1963), too. As an example of internal flow, there is the channel flow having a wave wall or a grooved wall (Nisimura et al., 1996). In this way, there are many researches concerning the body surfaces on which roughness and so on are continuously attached, but it seems that it is not clarified sufficiently, by paying attention to cavity itself, what influence is exerted to the boundary layer in the flows upstream and downstream of the cavity due to its shape.

Moreover, these studies are generally performed in the turbulent boundary layer. What kinds of effect happened to the laminar boundary layer by cavities are not clear sufficiently.

In this study, the shapes of cavities are changed into 3 kinds, rectangle, triangle and circular arc, and the depths of cavities are changed systematically, too. It is made clear, by numerical calculations and experiments, what states of flow are shown in the internal part of cavity and what kinds of influence are exerted to the laminar

boundary layer in the upstream and downstream flows.

2. Numerical Calculation

For executing calculation, the RNG (Renormalization Group) κ–ε turbulent model which is suitable to solve the problems of the flows accompanied by separating or circulating flow is employed (Yakuhot and Orszag, 1986; Choi, D. et al., 1994). Furthermore to make the calculation easier, the versatile thermal fluid analysis software Fluent/UNS is additionally used. As for the fluid to be dealt with, air is supposed, and its flow is assumed as 2-dimensional, incompressible, steady and free from the influence of external force. A continuity equation and Navier Stokes equation are the fundamental equations, and the equations shown below are obtained by applying ensemble average to these equations together with introduction of the RNG κ–ε model. The calculation conditions are listed in Table 1.

$$\frac{\partial u_i}{\partial x_i} = 0 \tag{1}$$

$$\frac{\partial}{\partial x_i}\left(\rho u_i \kappa\right) = \frac{\partial}{\partial x_i}\left[u_{\text{eff}}\left(\frac{\partial u_i}{\partial x_j} + \frac{\partial u_j}{\partial x_i}\right)\right] - \frac{\partial p}{\partial x_i} \tag{2}$$

$$\frac{\partial}{\partial x_i}\left(\rho u_i \kappa\right) = \frac{\partial}{\partial x_i}\left(\alpha_\kappa \mu_{\text{eff}} + \frac{\partial \kappa}{\partial x_i}\right) + \mu_t S^2 - \rho\varepsilon \tag{3}$$

$$\frac{\partial}{\partial x_i}\left(\rho u_i \varepsilon\right) = \frac{\partial}{\partial x_i}\left(\alpha_\varepsilon \mu_{\text{eff}} + \frac{\partial \varepsilon}{\partial x_i}\right) + C_{1\varepsilon}\frac{\varepsilon}{\kappa}\mu_t S^2 - C_{2\varepsilon}\rho\,\frac{\varepsilon^2}{\kappa} - R \tag{4}$$

$$S \equiv \sqrt{2 S_{ij} S_{ij}}$$

$$S_{ij} \equiv \frac{1}{2}\left(\frac{\partial u_i}{\partial x_j} + \frac{\partial u_j}{\partial x_i}\right)$$

$$R = \frac{C_\mu \rho \eta^3 \left(1 - \eta/\eta_0\right)}{1 + \beta\eta^3}\frac{\varepsilon^2}{\kappa}$$

$$\eta \equiv S\kappa/\varepsilon, \quad \mu_{\text{eff}} = \mu + \mu_t, \quad \mu_t = \rho C_\mu \kappa^2/\varepsilon, \quad \eta_0 \approx 4.38$$

$$\beta = 0.015, \quad C_\mu = 0.0845, \quad C_{1\varepsilon} = 1.42, \quad C_{2\varepsilon} = 1.68$$

Table 1. Computational conditions.

Turbulence model	RNG κ–ε
Reynolds number	$U_m \ L/\nu = 2.0 \times 10^5$
Initial velocity	20 m/s
Turbulence intensity	Experiment value (0.7%)
Grid number	3.0×10^4
Convergence judgment	1.0×10^{-4}
Boundary condition	
Inlet	Experiment value (U = 20 m/s)
Outlet	Experiment value
Wall	Non slip ($U = V$ = 0 m/s)
Computational domain	
X-direction	$-4.2 < x/c < 22.6$
Y-direction	$-k/c < y/c < 8.3$

Where u is flow velocity vector, p is pressure, κ is turbulent energy and ε is dissipation ratio of turbulent energy. Meanwhile, μ_{eff} is effective viscosity and is the sum of laminar flow viscosity μ and turbulence viscosity μ_t. In

addition, α_κ and α_ε are respectively the reciprocals of the turbulent Prantdl number concerning κ and ε.

3. Experimental Apparatus and Method

Figure 1 shows the cross-sectional shapes (Type A: circular arc, Type B: triangle and Type C: rectangle) of the cavity models used for this experiment. In this experiment, while letting the width of cavity be c and the depth be k for these shapes, the values of k/c are changed from 0 to 1. For these test models, the measurements of flow characteristics in the cavity and velocity distribution near the cavity are carried out. The entrance of cavity is set at the position of 150 mm from the leading edge of a plate as illustrated in Fig. 2. As the experiment is carried out at the constant flow velocity of 20 m/s, the laminar boundary layer will maintain about 380 mm length on the plate.

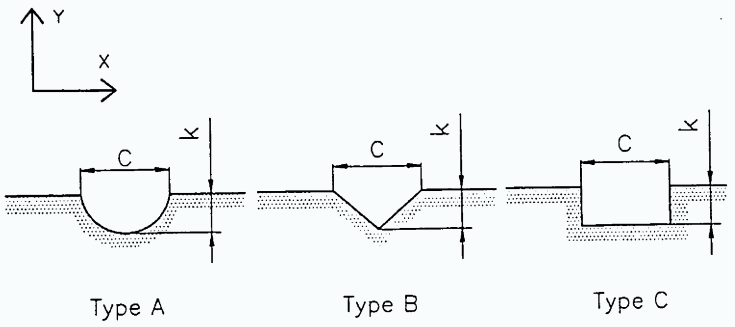

Fig. 1. Test model.

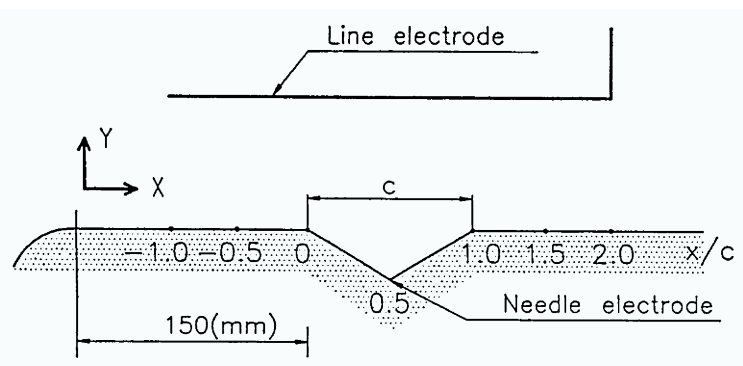

Fig. 2. Points of needle electrode.

So, it is clear that the cavity is set in the laminar boundary layer of a plate.

3.1 Measurement of the Flow Velocity Distribution

The experiment is performed using a suction type wind tunnel that has the square cross section with the width of 0.3 m and the length of 1.0 m. This wind tunnel has a test plate on the side that can be taken off as shown in Fig. 3. The constant temperature type hot-wire anemometer equipped with an X-type probe with 5 μm hot-wire is used for this experiment. The flow velocity is settled at 20 m/s. The output signals from the hot-wire anemometer are taken into a computer via A/D converter. From this computer, the component velocity of the time average flow velocity, turbulence intensity, shear stress, etc. can be outputted. The accuracy of this measurements of the velocity and the boundary layer thickness is about 5%.

3.2 Visualization Experiment by Spark Tracing Method

The co-ordinates of the test model and the setting positions of the electrodes are shown in Fig. 3 and 7 pieces tip-sharpened needle electrodes of 0.2 mm diameter are installed on the surface of the model. The wire electrodes of 1 mm diameter are placed parallel to the surface. The material of each electrode is tungsten wire. On the other hand, a high-voltage/high-frequency pulse generator is employed as the power source and the supplied voltage is adjusted to 90 kV, the pulse interval to 80 μs and the number of the pulses to 10.

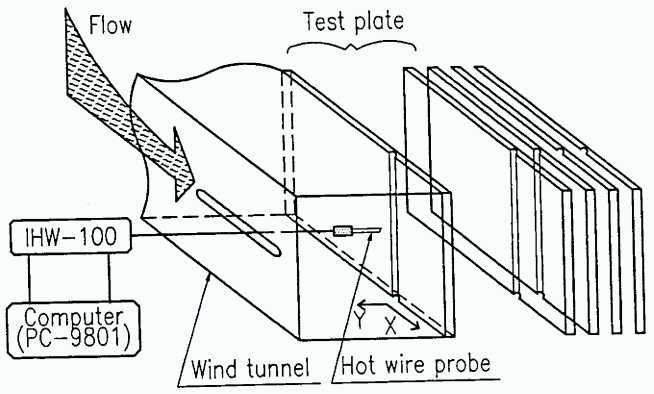

Fig. 3. Wind tunnel (measuring velocity).

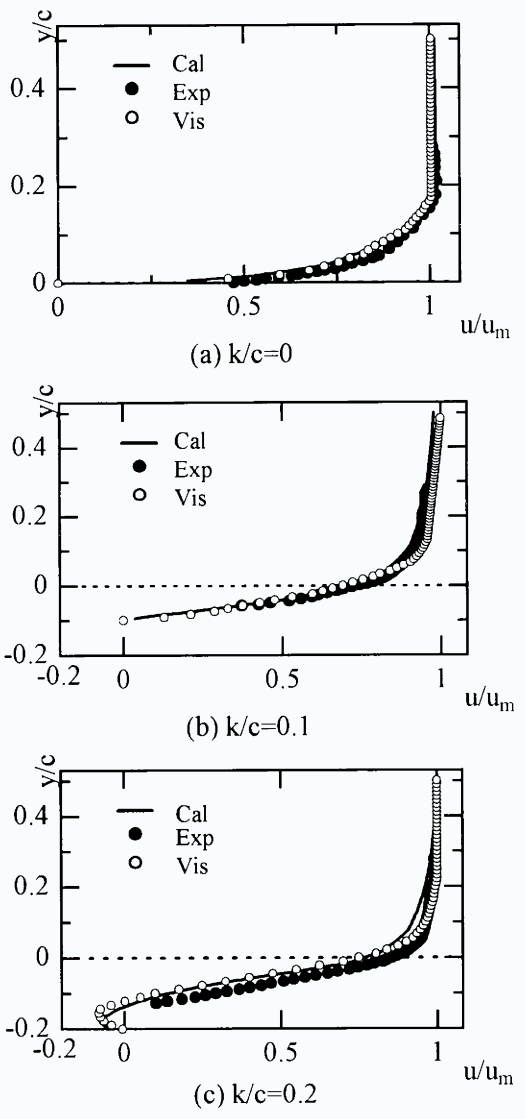

Fig. 4. Velocity distribution (Type B, $x/c = 0.5$)[Cal: Calculation, Exp: Experiments, Vis: Visualization].

4. Experimental Results and Consideration

4.1 Velocity Distribution on the Plates without and with Cavity

Figures 4(a), (b) and (c) show one example of the velocity distributions on the plates without and with cavity at the same position of cavity centre ($x/c = 0.5$). Figure 4(a) is for a flat plate and Figures (b), (c) are for the plates Type B with depths of $k/c = 0.1$, 0.2 respectively. In these figures, the experimental results of the hot-wire anemometer and visualization are compared with calculated results. These results agree well with each other. Figure 4 (b) shows that the reverse flow does not occur inside the cavity and air flows along to the cavity. However, Fig. 4 (c) shows that the reverse flow occurs inside the cavity.

Figures 5(a), (b) and (c) show the visualization results of spark tracing method photographed under the same conditions as those in Fig. 4. From Fig. 5(a), it is perceived that the thickness of the boundary layer increases

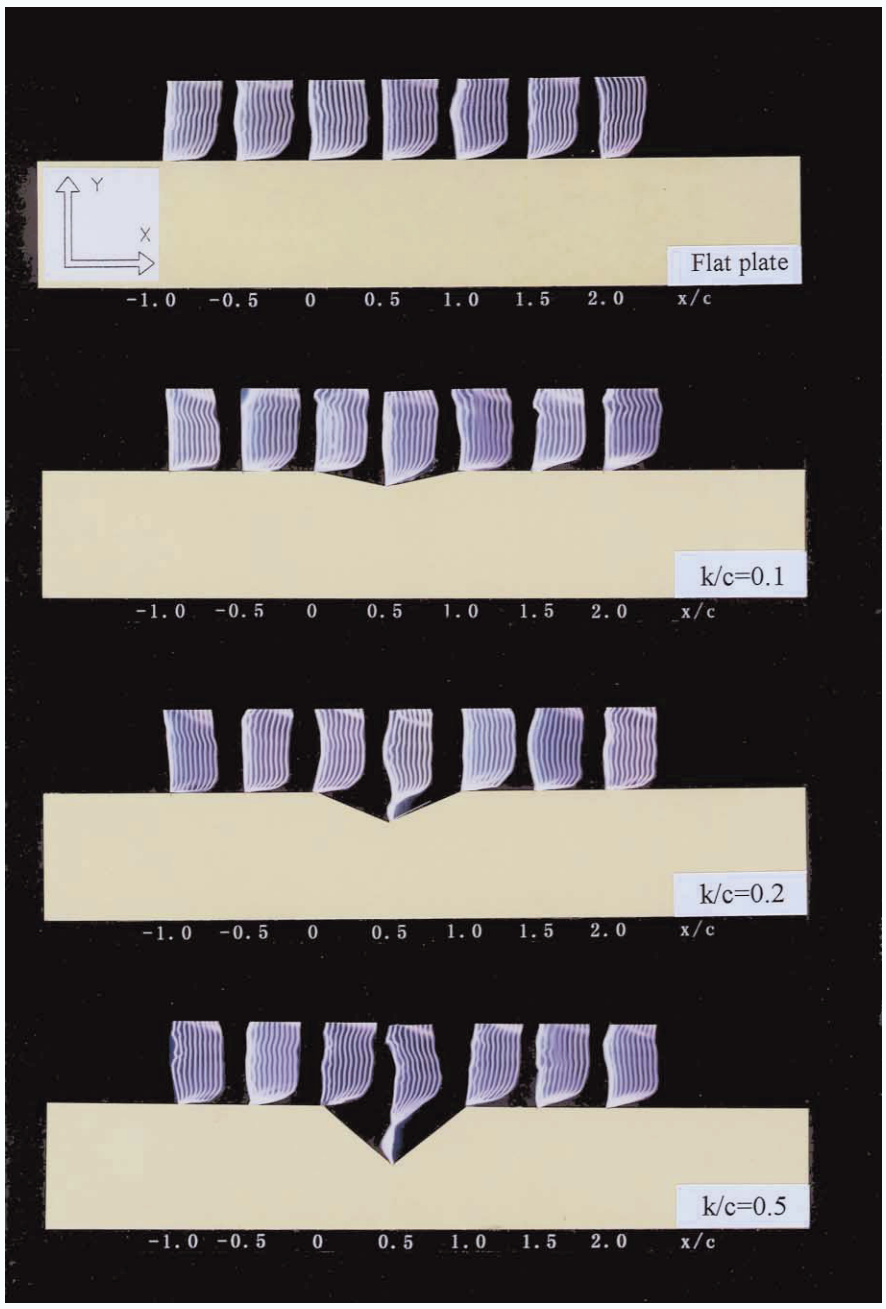

(a)

(b)

(c)

(d)

Fig. 5. The result of spark tracing method (Type B).

along to the flow on the plate. And the velocity distributions of the centre parts of the cavities agree with the results of Fig. 4.

4.2 Boundary Layer Thickness for the Shapes of Cavity

In Fig. 6, (a) (b) and (c) show the boundary layer thickness depended upon the difference in shapes at $k/c = 0.2$. The positions of measurement are at the centre of the cavity ($x/c = 0.5$) in the case of Fig. 6(a), at the outlet ($x/c = 1.0$) in the case of Fig. 6(b), and in the downstream region ($x/c = 1.5$) in the case of Fig. 6(c). From Fig. 6(a), it is found that the reverse flows occur in the cavities in any type at $x/c = 0.5$.

From the results of visualization, it is clear that the reverse flow occurs. The point that the value of u'/u becomes infinite is considered $u = 0$. So, this point is an inflection point. In this way, the negative velocity is obtained from the measuring values of hot-wire anemometer.

From Figs. 6(b) and (c), it is found that the boundary layer becomes thicker in the order of Types B, A, and C. From these results, it is observed that the triangle cavity suppresses the development of boundary layer.

Figures 7(a), (b) and (c) show the velocity distributions at the cavities outlet when the depths of cavities are changed to 0.1, 0.2, and 0.5. In these figures, the each boundary layer thickness δ is thinner than the boundary layer of a plate δ_m ($\delta/\delta_m < 1.0$) independent of the cavity shapes. Here, δ is the distance from the wall when the velocity reaches 99% of the velocity of the main flow above the plate.

In Fig. 8, (a)~(g) show the change of the boundary layer thickness by the change of the depths of the cavities at the points of $x/c = -1.38$~4.16. The horizontal axis shows the nondimensional depth of cavity (k/c), and the vertical axis shows the nondimensional boundary layer thickness (δ/δ_m).

From Fig. 8, it is clear that the boundary layer thickness of Types A, B and C does not differ from the

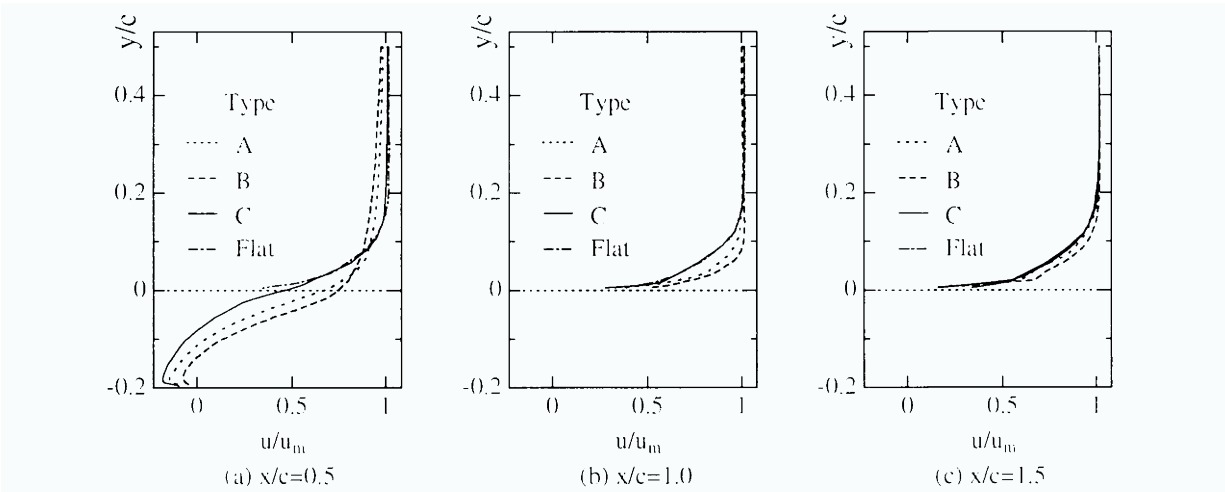

Fig. 6. Velocity distribution [$k/c = 0.2$].

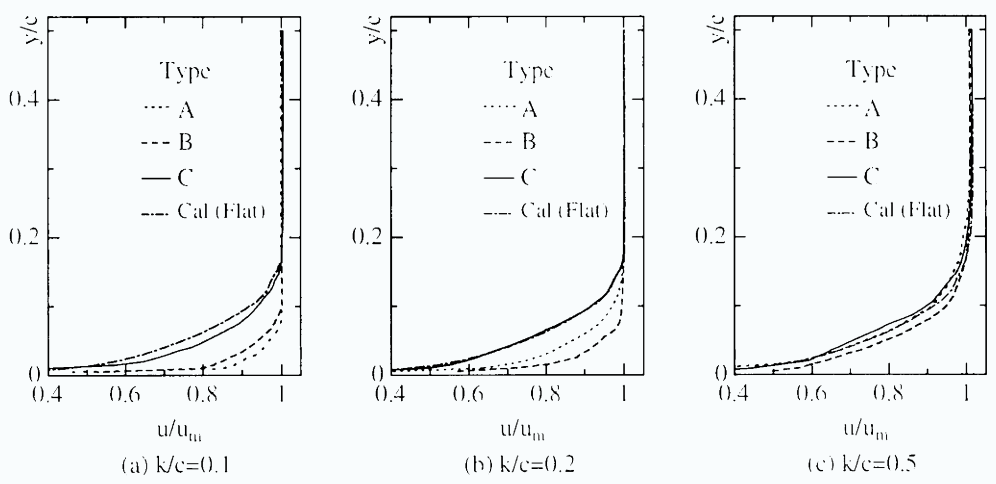

Fig. 7. Velocity distribution [$x/c = 1.0$, Cal: Calculation].

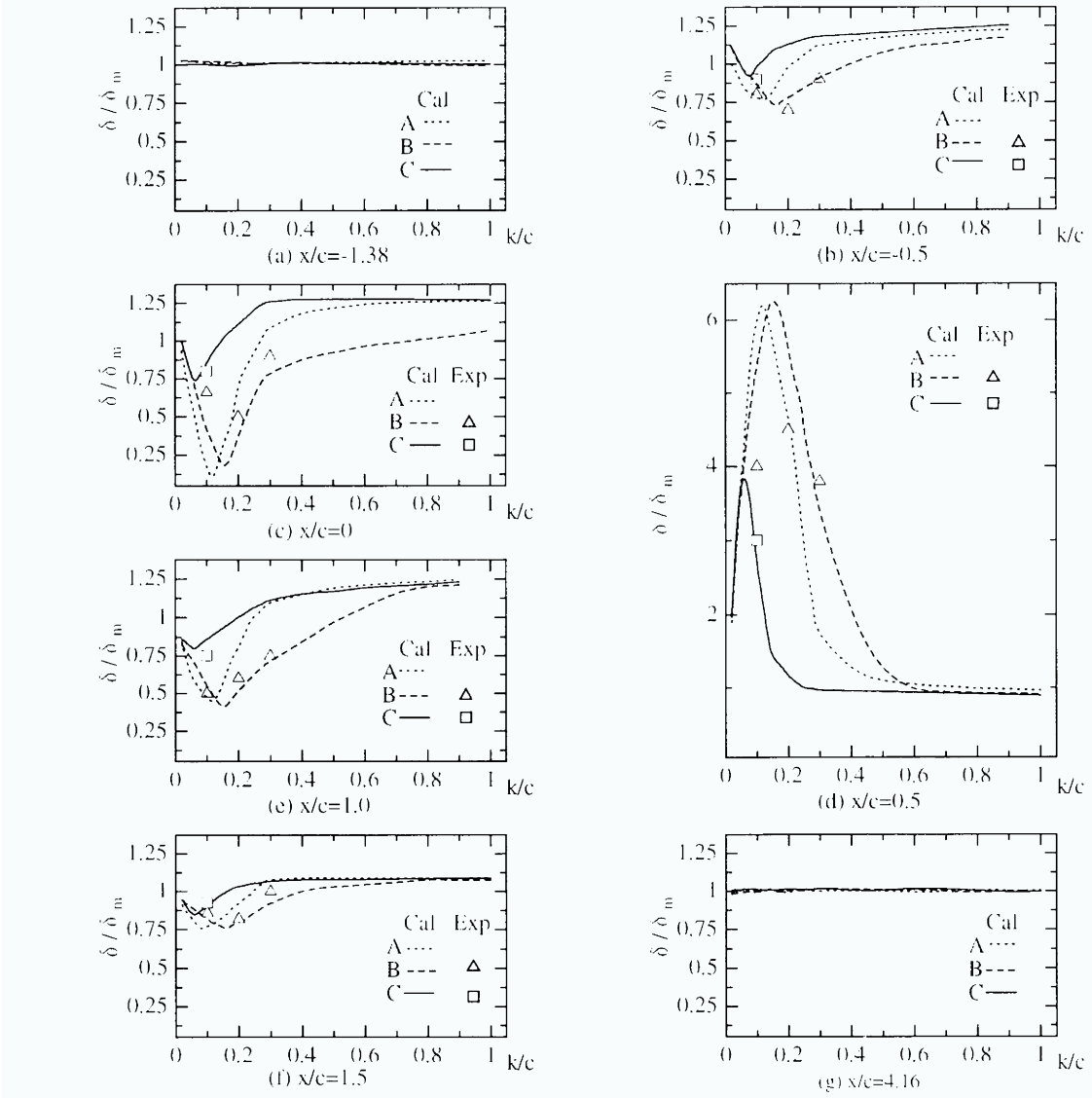

Fig. 8. Boundary layer thickness distribution [Cal: Calculation, Exp: Experiment].

boundary layer thickness of the flat plate at $x/c = -1.38$. However at $x/c = -0.5$, the boundary layer thickness near $k/c = 0.1$~0.2 is smaller than the boundary layer thickness of flat plate. In the case of k/c is very small or large, the values of δ/δ_m become larger than 1. From this facts, it is clear that the boundary layer thickness is influenced by the shape and depth of the cavities.

Still more approaching the cavity, this tendency becomes strong at the entrance of cavity as shown in Fig. 8 (c). But at the centre of cavity, the boundary layer thickness of any type becomes very large compared with that of flat plate and at over $k/c = 0.5$, it becomes almost equal flat plate as shown in Fig. 8(d).

Next, at the exit of cavity in Fig. 8(e), the boundary layer thickness becomes thin again. In the case of Type B, the boundary layer thickness becomes minimum at $k/c = 0.16$ and the values δ decrease till 42% compare with δ_m of the flat plate.

At the downstream region of the cavity in Fig. 8(f), the values of δ show the smaller minimum values according to the order of Types C, A and B and after that the values of δ increase. At k/c about over 0.3, the values of δ of any type are larger than the δ_m of flat plate and show almost constant values.

At the more down stream region in Fig. 8(g), the values of δ become equal to δ_m, so it seems that the influence of cavity does not reach there.

4.3 Flow Characteristic of the Cavity Inside

The aspects of changing the boundary layer thickness by the difference of k/c about Type B are shown in Figs. 9~11. Figure 9 shows velocity vector, Figure 10 streamline and Figure 11 pressure distribution. All (a)s in Figs. 9~11 with k/c = 0.04 indicate the states before the boundary layer thickness δ shows minimum value while (b)s with k/c = 0.16 are just showing minimum δ values. All (c)s and (d)s with k/c = 0.2, 0.5 show δ values increasing again.

In the case of Figs. (a), the air flows along to the surface of cavity and circulation is not generated. This is almost similar to the flow on the plate. However the boundary layer becomes thin at the inlet and exited parts of cavity. As these phenomena, the flow velocity increases as the pressure decreases at the entrance part of cavity, the velocity decreases as the pressure increases at the inside of cavity. And the velocity increases again as the pressure decreases at the exit part of the cavity. By these phenomena, it is considered that the boundary layer thickness decreases at the inlet and exited parts of cavities.

Figure 12 shows the velocity distribution of the x direction on the cavity at y/c = 0 for Type B. In case of k/c is small (k/c = 0.04), the velocity becomes high near the centre of cavity and approaches 0 at the entrance and exit parts of cavity. As against this, for k/c = 0.16 and 0.2 the velocity is constant at about 75% of main flow velocity and for k/c = 0.5 about 50% near entrance and exit of cavity. The velocity is zero at y/c = 0 for the flat plate, but for k/c = 0.16, 0.2 and 0.5, the velocity becomes large on the cavity. Especially for k/c = 0.5 that the reverse flow controls inside cavity, the flow separates at the entrance part of cavity, can not enter inside the cavity and becomes similar to the flow on the flat plate. For this reason the velocity on the cavity becomes lower compared with k/c = 0.16 and 0.2.

(a) k/c=0.04

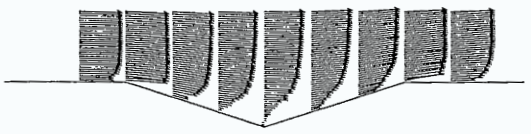

(b) k/c=0.16

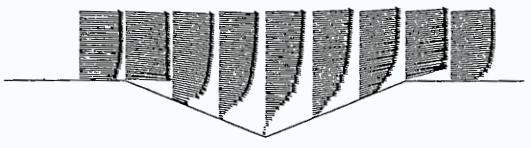

(c) k/c=0.20

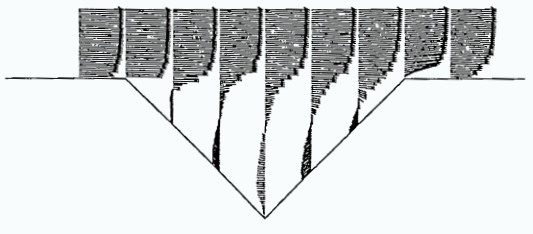

(d) k/c=0.50

Fig. 9. Velocity distribution (Type B).

(a) k/c=0.04

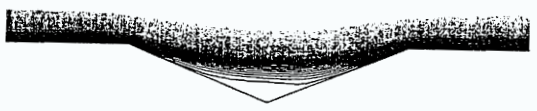

(b) k/c=0.16

(c) k/c=0.20

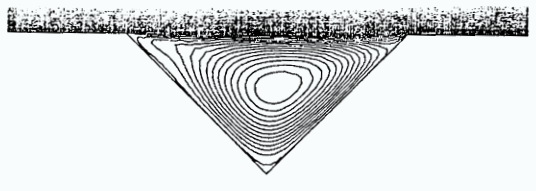

(d) k/c=0.50

Fig. 10. Stream line (Type B).

Figure 13 shows velocity distribution of x direction upon the cavity according to the shape difference on the case of $y/c = 0$ and $k/c = 0.2$. It is clear that the velocity becomes larger in order of Types C, A and B at any point of cavity. This agrees with the fact that the boundary layer thickness becomes thinner in order of Types C, A and B as shown in the results taken at inlet part (c) and exit part (e) of the cavity in Fig. 8.

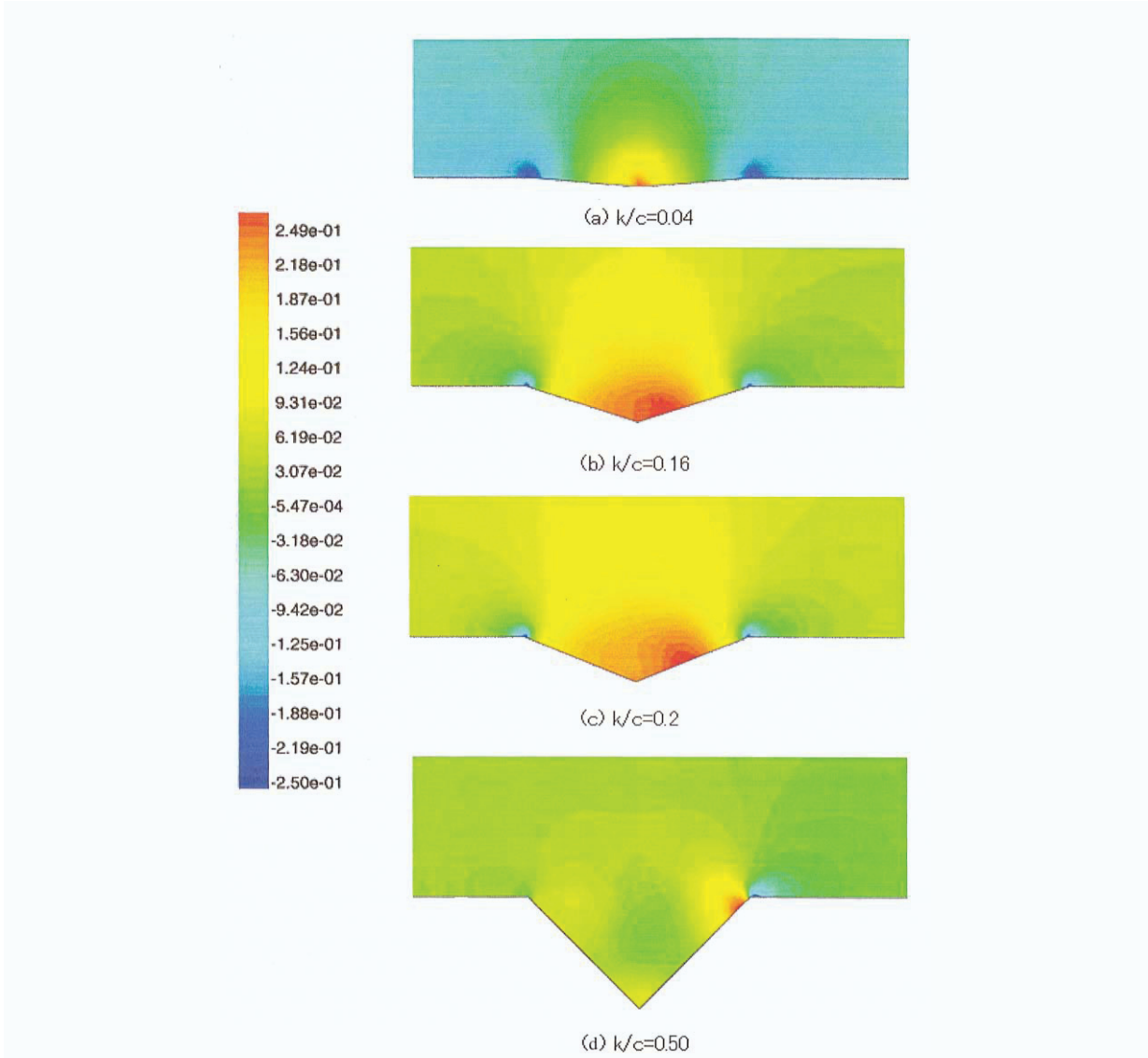

Fig. 11. Pressure distribution (Triangle Type).

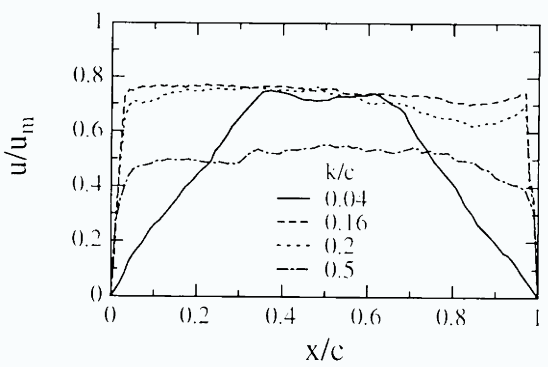

Fig. 12. Velocity distribution [$y/c = 0$, Type B].

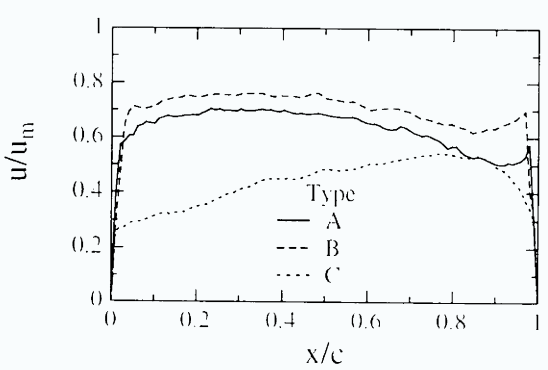

Fig. 13. Velocity distribution [$y/c = 0$, $k/c = 0.2$].

5. Conclusions

Triangle, square and circular arc cavities were formed on the plates, and the depth ratios (k/c) of these cavities were systematically changed and the characteristics of boundary layer was elucidated by means of numerical calculation and experiments. As the results, following matters were clarified.

1) By taking up adequately the depth ratios (k/c) of the cavities complying with the respective cavity shapes, the boundary layer thickness in the flows upstream and downstream of the cavities can be controlled. Also in whichever cavities, there are the minimum boundary layer thickness $(\delta/\delta_m)_{min}$ at certain depth ratios.
2) In whichever cavities, the development of boundary layer in the upstream and downstream regions can be suppressed in case that the depth ratios are small.
3) When the depth ratios of the cavities exceed certain values, the boundary layer thickness δ/δ_m becomes greater than 1. As the depth ratio becomes greater, it becomes constant value.
4) In case that the depth ratios k/c of the cavities are small, regardless of the cavity shapes, the boundary layer thickness (δ/δ_m) within the cavities takes the maximum value. In the triangular and arc cavities, the maximum boundary layer thickness $(\delta/\delta_m)_{max}$ reached the value as high as approximately 6.3 in the vicinity of $k/c = 0.2$.

References

Aihara, Y. et al., Applied Aerodynamics, 31-33, University of Tokyo (1991).
Aoki, K. et al., Flow Characteristics of a Golf Ball Using Visualization Techniques, Proceedings of the 1998 World Scientific Congress of Golf, Science and Golf 3 (1998), 446-456.
Choi, D. et al., Application of an RNG κ-ε Model to Compressible Turbulent Shear Layers, AIAA, Paper 94-00188 (1994).
Choi, K.-S., Near-wall structure of a turbulent boundary layer with riblets, J. Fluid Mech, 208(1989), 417-458.
Choi, K.-S. and Fujisawa, N., Possibility of drag reduction using d-type roughness, Applied Scientific Research, 50(1993), 315-324.
Maull, D. J. and East, L. F., Three-dimensional flow in cavities, J. Fluid Mech., 16(1963), 620-632.
Nisimura, T. et al., Flow Patterns and Wall Shear Stresses in Grooved Channels at Intermediate Reynolds Numbers, JSME, 62-598B(1996), 2106-2112.
Okajima, A. et al., Research Institute for Applied Mechanics, Reports, Kyushu University, No.40(1973), 387-400.
Perry, A. E. et al., Rough wall turbulent boundary layers, J. Fluid Mech., 37(1966), 383-413.
Tani, I. et al., Experimental Investigation of Flow Separation associated with a Step or a Groove, Aero. Res. Inst., Univ. of Tokyo, Report 364(1961), 119-137.
Townes, H. W. and Sabersky, R. H., Experiment on the Flow over a Rough Surface, Int. J. Heat Mass transfer, 9(1966), 729-738.
Yakuhot, V. and Orszag, S. A., Renormalizations Group Analysis of Turbulence, J. Sci. Comput., 1 (1986) , 3-51.

Author Profile

Katsumi Aoki: He received his M.Sc.(Eng.) degree in mechanical engineering in 1967 from Tokai University, and his Ph.D. in mechanical engineering in 1986 from the same University. After obtaining M.Sc. he worked as a research assistant, a lecturer, and an associate professor at Tokai University before, taking up his current position as a professor of Tokai University. His current research interests cover flow around a rotating circular cylinder with and without grooves, flow around a rotating sphere, possibility of drag reduction using triangle-type cavity, and flow visualization by spark tracing method of complicated flow field like in centrifugal blower.

Hiroo Okanaga: He received B.Sc.(Eng.) in mechanical engineering in 1985 from Faculty of Science and Technology, Keio University, and his Ph.D. in mechanical engineering in 1990 from the same University. After obtaining Ph.D. he worked as an assistant of Professor Aoki, before taking up his current position as an assistant Professor of the Tokai University. His research interests cover Electrohydrodynamics liquid jets which are produced by applying a high electric voltage between the ring electrode and plate electrode in the liquid as a mixture of R113 and ethanol.

Yasuki Nakayama: He received his B.Sc. (Eng.) degree in mechanical engineering in 1952 from Waseda University, and his Ph.D. in mechanical engineering from the same University in 1963. He joined the National Railway Research Institute and conducted many research investigations in the area of fluid mechanics. He then became a professor of Tokai University, where he taught and researched fluid mechanics and visualization. He later became President of the Future Technology Research Institute. He has received many distinctions and awards for his outstanding research. He has been a visiting professor of Southampton University, UK, President of The Visualization Society of Japan, and Director of the Japan Society of Mechanical Engineers. He has published 10 books and more than 160 research papers.